Tetrabutylammonium Salts of Aluminum(III) and Gallium(III) Phthalocyanine Radical Anions Bonded with Fluoren-9-olato(-) Anions and Indium(III) Phthalocyanine Bromide Radical Anions.

AUTHOR(S):

Konarev, Dmitri V; Khasanov, Salavat S; Ishikawa, Manabu; Nakano, Yoshiaki; Otsuka, Akihiro; Yamochi, Hideki; Saito, Gunzi; Lyubovskaya, Rimma N

CITATION:

Konarev, Dmitri V ...[et al]. Tetrabutylammonium Salts of Aluminum(III) and Gallium(III) Phthalocyanine Radical Anions Bonded with Fluoren-9-olato(-) Anions and Indium(III) Phthalocyanine Bromide Radical Anions.. Chemistry - an Asian journal 2017, 12(8): 910-919

ISSUE DATE:

2017-04-18

URL:

http://hdl.handle.net/2433/224817

Tetrabutylammonium salts of aluminum(III) and gallium(III) phthalocyanine radical anions bonded with fluoren-9-olato⁻ anions and indium(III) bromide phthalocyanine radical anions

Dmitri V. Konarev,*[a] Salavat S. Khasanov,[b] Manabu Ishikawa,[c, d] Yoshiaki Nakano,[c] Akihiro Otsuka,[c] Hideki Yamochi,[c] Gunzi Saito[e] and Rimma N. Lyubovskaya[a]

[a] Dr. D. V. Konarev, Prof. R. N. Lyubovskaya,
Institute of Problems of Chemical Physics RAS, Chernogolovka, Moscow region, 142432 Russia, konarev3@yandex.ru.

[b] Dr. S. S. Khasanov
Institute of Solid State Physics RAS, Chernogolovka, Moscow region, 142432 Russia.

[c] Dr. M. Ishikawa, Dr. Y. Nakano, Dr. A. Otsuka, Prof. H. Yamochi
Division of Chemistry, Graduate School of Science, Kyoto University, Sakyo-ku, Kyoto 606-8502, Japan.

[d] Dr. M. Ishikawa,
Research Center for Low Temperature and Materials Sciences, Kyoto University, Sakyo-ku, Kyoto 606-8501, Japan.

[e] Prof. G. Saito
Faculty of Agriculture, Meijo University, 1-501 Shiogamaguchi, Tempaku-ku, Nagoya 468- 8502, Japan.
Toyota Physical and Chemical Research Institute, 41-1, Yokomichi, Nagakute, Aichi 480-1192, Japan.

Supporting information for this article is given via a link at the end of the document.

Abstract: Reduction of aluminum(III), gallium(III) and indium(III) chloride phthalocyanines by sodium fluorenone ketyl in the presence of tetrabutylammonium cations yielded crystalline salts $(Bu_4N^+)_2[M^{III}(HFl{-}O^-)(Pc^{\bullet 3-})]^{\bullet-}(Br^-)\cdot 1.5C_6H_4Cl_2$ (M = Al (**1**), Ga(**2**), HFl–O$^-$ = Fluoren-9-olato$^-$ anion) and $(Bu_4N^+)[In^{III}Br(Pc^{\bullet 3-})]^{\bullet-}\cdot 0.875C_6H_4Cl_2\cdot 0.125C_6H_{14}$ (**3**). The salts contain $Pc^{\bullet 3-}$ radical anions with negatively charged phthalocyanine macrocycles evidenced by the presence of intense bands of $Pc^{\bullet 3-}$ in the NIR range and noticeable blue shift of both Q- and Soret bands of phthalocyanine. The metal(III) atoms coordinate HFl–O$^-$ anions in **1** and **2** with short Al-O and Ga-O bonds of 1.749(2) and 1.836(6) Å, respectively. The HFl–O$^-$ anions have longer C-O bonds (1.402(3) and 1.391(11) Å, respectively) than those observed for fluorenone ketyl (1.27-1.31 Å). Salts **1**-**3** show effective magnetic moments of 1.72, 1.66 and 1.79 μ_B at 300 K due to the presence of unpaired S = 1/2 spins on $Pc^{\bullet 3-}$. These spins are coupled antiferromagnetically with Weiss temperatures of -22, -14 and -30 K for **1**-**3**, respectively. Coupling can occur in the corrugated two-dimensional phthalocyanine layers of **1** and **2** with exchange interaction of J/k_B = -0.9 – -1.1 K and π-stacking $\{[In^{III}Br(Pc^{\bullet 3-})]^{\bullet-}\}_2$ dimers of **3** with exchange interaction of J/k_B = -10.8 K. The salts show intense EPR signals attributed to $Pc^{\bullet 3-}$. It was found that increasing size of central metal atom strongly broadens these EPR signals.

Introduction

Metal phthalocyanine (MPc) in radical cation or radical anion state can show promising magnetic and conducting properties.[1-20] For example, electrochemical or chemical oxidation of neutral M^{II}Pc's or electrochemical oxidation of the $\{M^{III}(CN)_2Pc\}^-$ anions allow the preparation of compounds with metallic conductivity which in some cases is stable down to liquid helium temperatures.[1-3] Oxidation of unsubstituted and substituted manganese(II) phthalocyanines by organic π-acceptor tetracyanoethylene yields coordination chain compounds with ferrimagnetic ordering of spins.[4, 5]

Reduction of MPc's is also intensively studied.[6-18] Interest to this field is evoked by the prediction of metallic conductivity or superconductivity in electron doped MPc's[21] and the observation of ferrimagnetic ordering of spins in $(Cp^*_2Cr^+)[Fe^I(Pc^{2-})]^-\cdot 4C_6H_4Cl_2$ with chains of alternating iron(I) phthalocyanine anions (Fe^I, S = 1/2) and decamethylchromocenium cations (Cr^{III}, S = 3/2)[22]. Up to now, several types of anionic metal phthalocyanines were obtained as crystals and structurally characterized. A series of the $(C^+)[M(Pc^{\bullet 3-})]^{\bullet-}$ salts (M = H_2, Ni^{II}, Cu^{II}, Pb^{II}, Sn^{II}, $Ti^{IV}O$, $V^{IV}O$, $Sn^{IV}Cl_2$) with tetraalkylammonium cations (C^+) was obtained allowing the analysis of properties of metal phthalocyanines with the reduced phthalocyanine macrocycle in solid state[6-8]. Reduction is also centered on the phthalocyanine macrocycle in $[(K^+)_2(DME)_4][Mg^{II}(OH^-)(Pc^{\bullet 3-})]^{\bullet-}$ (DME is 1,2-dimethoxyethane), $[M^{III}(MeIm)_2(Pc^{\bullet 3-})]^{\bullet}$ (M = Al^{III}, Ga^{III}, MeIm is *N*-methylimidazole),

$[Al^{III}(anisole)_2(Pc^{\bullet 3-})]^{\bullet}$, $[Sn^{IV}Ph(Pc^{\bullet 3-})]^{\bullet}$, $Ge^{IV}(Pyridine)_2(Pc^{4-})$ and $K_2Nb^{IV}O(Pc^{4-})\cdot 5DME$ containing radical trianion (•3–) and tetraanion (4–) phthalocyanine macrocycles[9-14]. Reduction of iron and cobalt phthalocyanines is centered on the metal atoms forming the $[Fe^{I}(Pc^{2-})]^{-}$, $[Co^{I}(Pc^{2-})]^{-}$ and $[Fe^{0}(Pc^{2-})]^{2-}$ anions[15-18]. Iron(II) hexadecachlorophthalocyanine forms salts with effective π-π stacking or a layered arrangement of phthalocyanine macrocycles[19, 20].

In the studies of metal phthalocyanine reduction by sodium fluorenone ketyl in the presence of tetrabutylammonium cations, we found that generally metal phthalocyanine radical anions $[M^{II}(Pc^{\bullet 3-})]^{\bullet -}$ are formed which can be crystallized as tetraalkylammonium salts [6]. Contrary, the reduction of aluminum(III) and gallium(III) chloride phthalocyanines in the same conditions results in the chloride anion substitution at the metal(III) atoms by the fluoren-9-olato^{-} anions (HFl–O^{-}). This ability is explained by high affinity of these metals to oxygen containing ligands. Previously coordination complex of such type was obtained with boron subphthalocyanine. Coordinated fluorenone ketyl dimerized in this complex to form dimeric $[(B^{III}SubPc^{+})_2(Fl\text{-}O^{-})_2]$ species which were cocrystallized with fullerene C_{60}.[23] Indium(III) chloride phthalocyanine does not tend to coordinate the HFl–O^{-} anions and instead of that chloride anions are substituted by bromine anions at the indium(III) atoms to form the $[In^{III}Br(Pc^{\bullet 3-})]^{\bullet -}$ radical anions. In this work we discuss crystal structures, optical and magnetic properties of the $(Bu_4N^{+})_2[M^{III}(HFl\text{–}O^{-})(Pc^{\bullet 3-})]^{\bullet -}(Br^{-})\cdot 1.5C_6H_4Cl_2$ (M = Al (**1**), Ga (**2**)) and $(Bu_4N^{+})[In^{III}Br(Pc^{\bullet 3-})]^{\bullet -}\cdot 0.875C_6H_4Cl_2\cdot 0.125C_6H_{14}$ (**3**) salts which are paramagnetic due to the presence of spin on the $Pc^{\bullet 3-}$ macrocycle and show magnetic exchange interactions.

Results and discussion

a. Synthesis.

Salts **1** and **2** were synthesized in pure *o*-dichlorobenzene by the reduction of $Al^{III}Cl(Pc^{2-})$ and $Ga^{III}Cl(Pc^{2-})$ with an excess of sodium fluoreneone ketyl in the presence of an excess of tetrabutylammonium bromide, respectively. The reaction mixture is turned to a deep blue solutions, which is the characteristic color for reduced phthalocyanine macrocycles.[6] Additionally, chloride anions bonded to metal(III) atoms were substituted with fluorenone forming new coordination assemblies. When the coordination unit contains Fl=O$^{\bullet -}$ (Fl=O: Fluorenone ketyl), $Pc^{\bullet 3-}$ can show strong magnetic coupling with this paramagnetic species. However, structural, optical and magnetic properties of both salts indicate the presence of diamagnetic fluoren-9-olato^{-} (HFl–O^{-}) anion which is the deprotonated anion of fluorenol – alcohol derivative of fluorene (possibly the Fl=O$^{\bullet -}$ radical anions abstract hydrogen atoms from solvent molecules). The singly bonded ketyl dimers $(Fl\text{–}O^{-})_2$ [23, 24] are

not formed in **1** and **2**. In contrast to $Al^{III}Cl(Pc^{2-})$ and $Ga^{III}Cl(Pc^{2-})$, the $HFl–O^-$ anion is not coordinated to the indium(III) atoms of $In^{III}Cl(Pc^{2-})$. Instead of that, chloride anion at In^{III} is substituted with the bromide anions originated from $(Bu_4N^+)(Br^-)$ used in excess in the synthesis. Previously substitution of Cl^- by Br^- was found in the tetrabutyl- and tetraethylammonium salts containing indium(III) bromide phthalocyanine and fullerene C_{60} radical anions. The starting compound in this synthesis was also $In^{III}Cl(Pc^{2-})$.[25]

b. Optical properties.

The spectra of starting $Al^{III}Cl(Pc^{2-})$ and salt **1** in KBr pellets are shown in Fig. 1a. The spectrum of $Al^{III}Cl(Pc^{2-})$ shows the typical feature of metal phthalocyanines in solid state exhibiting the split Q-band positioned in the visible range at 647, 715 (maximum) and 811 nm and the Soret band positioned at 356 nm. The formation of **1** strongly affects the optical spectrum. An intense band is manifested in the NIR range at 1001 nm and essentially weaker bands can be found at 924 and 843 nm (Fig. 1a). The lowest energy band is attributed to $Pc^{\bullet 3-}$ and these bands can be found in the spectra of all metal phthalocyanines with the reduced phthalocyanine macrocycle. The transition energy of this NIR absorption band is slightly affected by the central metal atom and shifts from 920 (Cu^{II}) to 1040 nm (Sn^{II}).[6] The $[Fe^{I}(Pc^{2-})]^-$ and $[Co^{I}(Pc^{2-})]^-$ anions with the reduced central metals do not show such bands.[17-20] Reduction of the Pc macrocycle in **1** strongly blue shifts the Q and Soret bands of phthalocyanine which are manifested as a split band at 590 and 629 nm in the visible range and a single band at 334 nm in the UV range, respectively. Such shifts are observed in the salts with $[M(Pc^{\bullet 3-})]^{\bullet -}$ (M = H_2, Ni^{II}, Cu^{II}, Pb^{II}, Sn^{II}, $Ti^{IV}O$, $V^{IV}O$, $Sn^{IV}Cl_2$).[6-8] Similar behavior is demonstrated by salts **2** and **3** (Fig. 1b and 1c, respectively). Starting $Ga^{III}Cl(Pc^{2-})$ has the position of the Q- and Soret bands in the spectrum at 664, 715 (maximum) and 343 nm, whereas the positions of these bands for $In^{III}Cl(Pc^{2-})$ are at 666, 727 (maximum) and 372 nm, respectively. As in **1**, the formation of **2** and **3** is accompanied by the appearance of new bands in the NIR range at 1007 and 1013 nm, respectively and strong blue shifts of the Q and Soret bands to 594, 627 and 330 nm (**2**) and 596, 634, 704 and 335 nm (**3**). Such changes can be attributed to the formation of $Pc^{\bullet 3-}$.

IR-spectra of starting phthalocyanines and salts **1**-**3** in KBr pellets are shown in Supporting information (Table S1 and Figs. S1-S3). The absorption bands of all the components can be found in the spectra of the salts with small shift (up to 8 cm^{-1}) relative to the starting compounds. The formation of **1** and **2** affects the spectrum of starting fluorenone ketyl radical anions whose spectrum was obtained for the $(Na^+)(Fl{=}O^{\bullet -})$ salt. The intense C=O stretching mode bands at 1609 and 1674 cm^{-1} observed for sodium fluorenone ketyl salt are disappeared, which is regarded as the result of the conversion of double

C=O bond in Fl=O$^{\bullet-}$ to a single C-O bond in the HFl–O^{-} anion. A similar spectrum is observed for **3** excepting the absorption bands of the HFl–O^{-} anions.

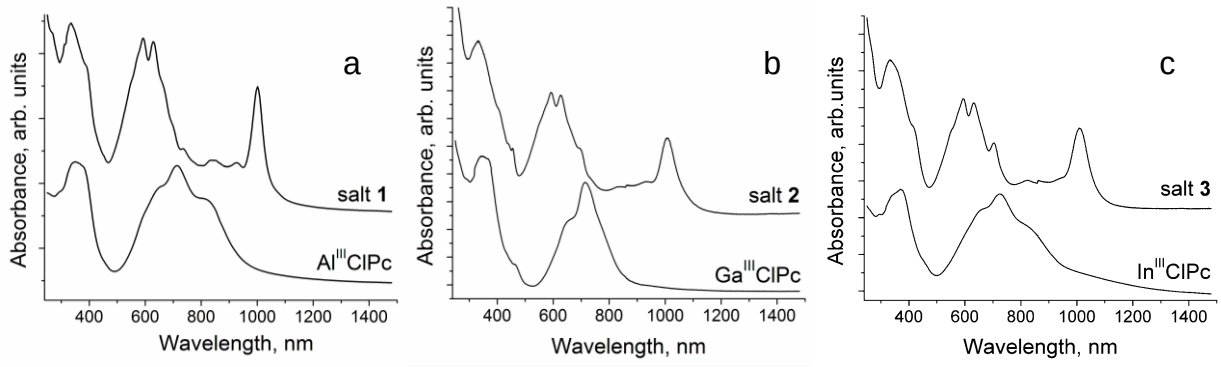

Fig. 1. Spectra of starting metal(III) chloride phthalocyanine and salts **1** (a); **2** (b) and **3** (c) in the UV-visible-NIR range measured at room temperature in KBr pellets prepared for salts in anaerobic conditions.

c. Crystal structures

Salts **1** and **2** are isostructural and have monoclinic unit cell (Fig. 2a). There are two Bu_4N^+ cations and one Al^{3+} per formula unit. The +5 charge is compensated by one bromine Br^- anion, one HFl–O^{-} anion and phthalocyanine macrocycle having –3 charge to be in the radical trianion Pc$^{\bullet3-}$ state. Unusual feature of both salts is the presence of *p*-dichlorobenzene molecules in one position of **1** with the 0.5 occupancy and in one position of **2** with the 0.356(4) occupancy. Since isomerically pure *o*-dichlorobenzene was used in the synthesis, it is most plausible that Al^{III}Cl(Pc^{2-}) and Ga^{III}Cl(Pc^{2-}) play a role of catalyst for isomerization of *o*-dichlorobenzene since $AlCl_3$ is known to isomerize *o*-dichlorobenzene to *p*-dichlorobenzene[26]. It is seen that Ga^{III}ClPc is less effective than Al^{III}ClPc and In^{III}ClPc is ineffective for isomerization *o*-dichlorobenzene since in case of **2** mixture of *p*- and *o*-dichlorobenzene molecules is formed but only *o*-dichlorobenzene molecules are found in **3**. Other metal phthalocyanine [M(Pc$^{\bullet3-}$)]$^{\bullet-}$ salts (M = Sn^{II}, Pb^{II}, Ti^{IV}O, Sn^{IV}Cl$_2$) also contain only *o*-dichlorobenzene molecules.[6-8]

Geometric parameters of aluminum(III) and gallium(III) phthalocyanines in **1** and **2** are listed in Table 1. Since geometry of Al^{III}Cl(Pc^{2-}) is unknown and structure of Ga^{III}Cl(Pc^{2-}) is determined only by the Rietveld method,[33] it is impossible to determine correctly how reduction affects geometry of Al^{III}ClPc and Ga^{III}ClPc. The average M^{III}-N(Pc) bonds are shorter for Al^{III} (1.975(3) Å) than for Ga^{III} (1.996(7) Å). As a result, the Al^{III} atoms have slightly smaller displacement from the 24-atom Pc plane than the Ga^{III} atoms (0.518 *vs* 0.534 Å, respectively). The metal(III) atoms come out of the Pc plane due

to coordination of bulky HFl–O$^-$ anions (Fig. 2a). The Al^{III}-O and Ga^{III}-O bond lengths are only 1.749(2) and 1.836(6) Å, respectively. Such length is typical for coordination compounds of Al^{III} and Ga^{III} with oxygen containing fluorenone based ligands (see Table 1).

Neutral 9-fluorenone and fluorenone ketyl radical anions are nearly planar with the maximal deviation of oxygen atom from the 13-atom fluorenone plane by 0.136 Å (Table 1). The C=O bond length in these units is close to the length of normal double C=O bonds. The length is 1.22-1.28 Å for neutral 9-fluorenone and 1.27-1.31 Å for the fluorenone ketyl radical anions (Table 1). The C-O bonds essentially elongated to 1.41-1.44 Å in the HFl-O$^-$ anions or dimeric fluorenone ketyls (Table 1). As a result, oxygen atoms distinctly deviate from the 13-atom fluorenone plane, namely, by 0.77-1.07 and 0.78-1.02 Å, respectively. The geometry of fluorenone units in **1** and **2** shows the strong deviation of oxygen atoms from the 13-atom fluorenone plane by 0.84-0.85 Å and essential elongation of the C-O bonds up to 1.38-1.40 Å, and hence it is concluded that HFl–O$^-$ anions are formed in these salts (Table 1).

The main structural motif of salts **1** and **2** is chains composed of the [M^{III}(HFl–O$^-$)(Pc$^{\bullet 3-}$)]$^{\bullet -}$ radical anions and channels formed by four TBA$^+$ cations occupied by two Br$^-$ anions, both are arranged along the *a*-axis (Fig. 3a). The planes of HFl–O$^-$ anions in these chains are nearly parallel and locate close to each other, and the dihedral angle between the planes is close to 0^o and the interplane distance is 3.56 Å (Fig. 3c). Phthalocyanine chains are arranged in a crystal in such a way that Pcs from different chains form corrugated nearly square layers parallel to the *ab* plane (Fig. 3b). There are several short side-by-side van der Waals C,N···C,N contacts between Pcs in these layers which are shown by green dashed lines in Fig. 3b.

In contrast to Al^{III}ClPc and Ga^{III}ClPc, In^{III}ClPc is not coordinated by the HFl-O$^-$ anions. In this case, chloride anion is substituted by bromide anion during the reduction in the presence of an excess of (Bu$_4$N)Br to form [In^{III}Br(Pc$^{\bullet 3-}$)]$^{\bullet -}$. Due to larger size of indium(III) atom, it shows the strong shift by 0.77-0.81 Å from the 24-atom Pc plane. The average length of the In-N(Pc) bonds of 2.11-2.12 Å is essentially longer than those for Al^{III} and Ga^{III}Pc (Table 1).

The phthalocyanine macrocycle has longer and shorter N-C bonds with pyrrole and imine nitrogen atoms. There is no alternation of these bonds in the –2 charged macrocycles. Longer C-N$_{pyr}$ bonds are not alternated in **1**-**3** (Table 1). Changes in the C-N$_{imine}$ bonds are within the experimental error for **1** and **2**. Noticeable alternation of these bonds is only found in **3** (Table 1). This alternation is realized by such a way that four bonds belonging to two oppositely located isoindole units are longer than four other bonds belonging to two different oppositely located isoindole units. Such alternation is characteristics of

$Pc^{\bullet 3-}$ and is observed due to partial disruption of aromaticity of the Pc macrocycle at the transition from stable 18-π-electron system of Pc^{2-} to less stable 19-π-electron system of $Pc^{\bullet 3-}$.[6-8]

The $[In^{III}Br(Pc^{\bullet 3-})]^{\bullet -}$ radical anions form π-stacking $\{[In^{III}Br(Pc^{\bullet 3-})]^{\bullet -}\}_2$ dimers in **3**. View on this dimer along the In-Br

bond is shown in Fig. 4a. The Pc macrocycles are strongly shifted in these dimers in such a way that isoindole unit of one phthalocyanine is positioned over the half of the 24-atom Pc macrocycle of neighboring Pc. Interplanar distance in this case is 3.23 Å, and 10 short van der Waals C,N···C,N contacts are formed within the dimers (Fig. 4b). Crystal structure of **3** is shown in Fig. 4b. It contains the alternating layers of $\{[In^{III}Br(Pc^{\bullet 3-})]^{\bullet -}\}_2$ dimers and TBA^+ along the *c*-axis (Fig. 4b). The anionic dimers are isolated from each other and have no short van der Waals contacts with the neighboring ones (Fig. 4b).

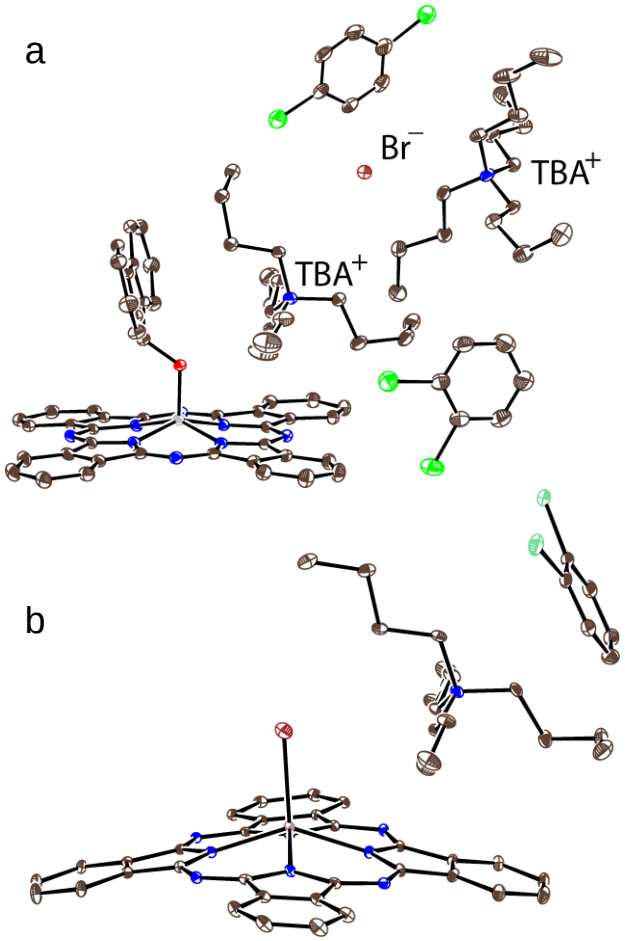

Fig. 2. Independent components in the crystal structure of: (a) salt **1** (the same for **2**) and (b) **3**. Ellipsoids are shown with the 30% probability. Disordered components are shown in the major occupied orientation.

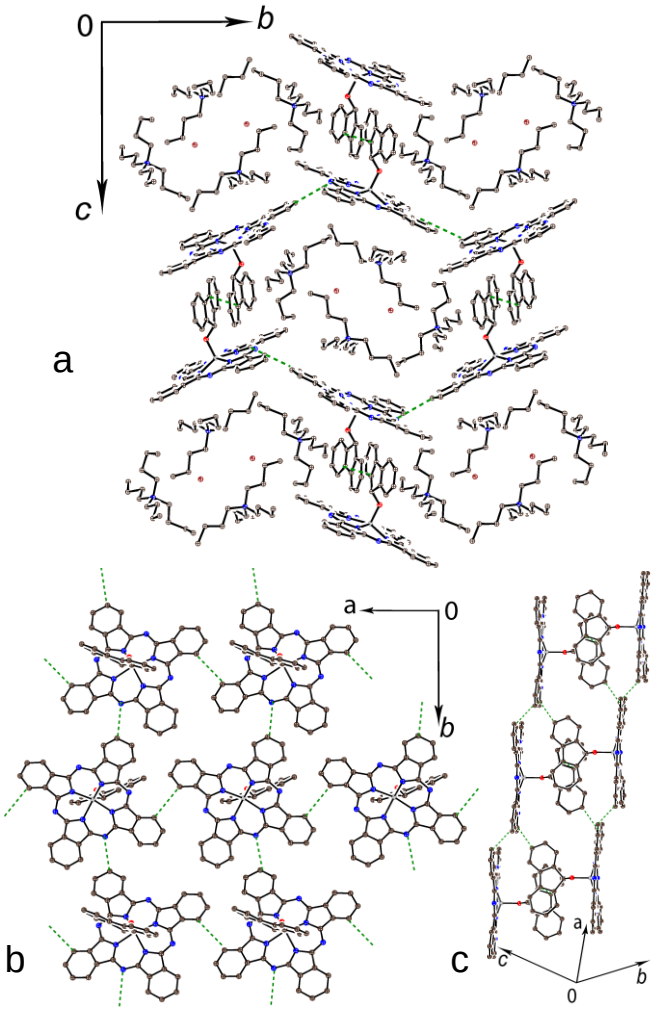

Fig. 3. Crystal structure of **1**: (a) view along the *a* axis and phthalocyanine layers; (b) view on the phthalocyanine layers positioned parallel to the *ab* plane; (c) view on phthalocyanine chains arranged along the *a* axis. Solvent molecules are not shown for clarity. The van der Waals C,N···C,N contacts between phthalocyanines shorter than 3.56 Å are shown by green dashed lines. Salt **2** has similar structure.

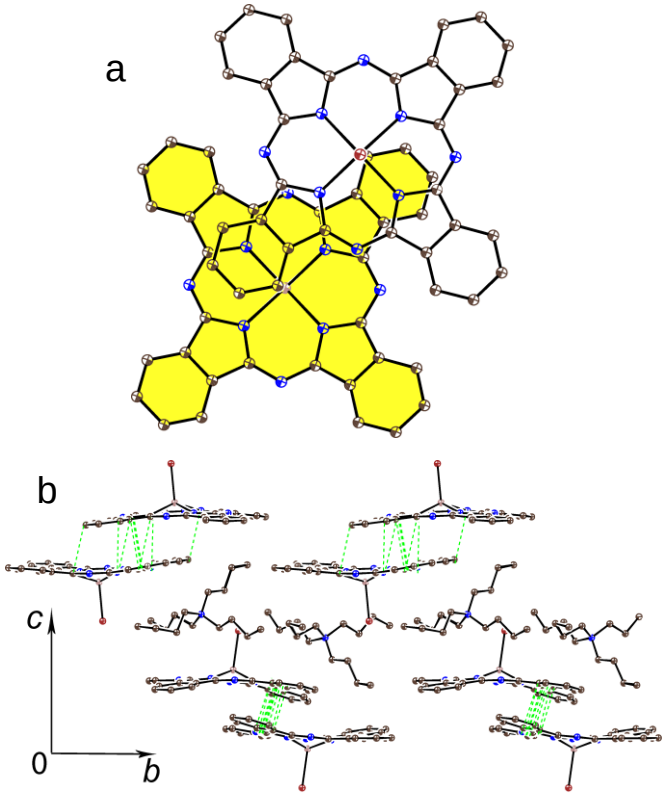

Fig. 4. a). View on the $\{[In^{III}Br(Pc^{\bullet 3-})]^{\bullet -}\}_2$ dimer along the In-Br bond. The most distant of the two Pc macrocycles is shown by yellow color; b). Layers from the $\{[In^{III}Br(Pc^{\bullet 3-})]^{\bullet -}\}_2$ dimers are positioned in the *ab* plane. The van der Waals C,N···C,N contacts between phthalocyanine macrocycles are shown by green dashed lines.

Table 1. Geometric parameters of phthalocyanine macrocycle and fluorenone units in salts **1**-**3** and those of reference compounds containing neutral fluorenone, the HFl−O$^-$ anions and monomeric and dimeric fluorenone ketyls.

Compound	Geometry of phthalocyanine				Geometry of fluorenone units	
	M-N(Pc), Å	Deviation of M from 24-atom Pc plane	M-O(Fluor), Å	N_{py}-C, Å N_{im}-C, Å short/long difference	C-O, Å	Deviation of O atoms from 13-atom fluorene plane
{(BSubPc)$_2$(Fl-O$^-$)$_2$}·C_{60}·2$C_6H_4Cl_2$ (fluorenone ketyl dimer)[23]	1.503(5)	-	1.426(4) 1.436(5)	1.366(4) 1.344(4)	1.423(4) 1.434(4)	0.924 1.075
(Bu_4N^+)$_2$[Al^{III}(HFl–O$^-$)($Pc^{\bullet 3-}$)]$^{\bullet-}$(Br^-)·1.5$C_6H_4Cl_2$ (**1**), (fluoren-9-olato$^-$ anion)	1.975(3)	0.518	1.749(2)	1.388(4) 1.327(4)/ 1.328(4) 0.001	1.402(3)	0.836
(Bu_4N^+)$_2$[Ga^{III}(HFl–O$^-$)($Pc^{\bullet 3-}$)]$^{\bullet-}$(Br^-)·1.5$C_6H_4Cl_2$ (**2**), (fluoren-9-olato$^-$ anion)	1.996(7)	0.534	1.836(6)	1.382(11) 1.315(11)/ 1.336(11) 0.021	1.391(11)	0.853
(Bu_4N^+)[$In^{III}Br$($Pc^{\bullet 3-}$)]$^{\bullet-}$·0.875$C_6H_4Cl_2$·0.125C_6H_{14} (**3**) 2 independent units	2.123(4)	0.812	In-Br 2.5280(8)	1.384(6) 1.319(6)/1.366(6) 0.047	-	-
	2.115(4)	0.772	2.5180(8)	1.383(6) 1.323(6)/1.357(6) 0.034		
9-fluorenone[27]	-				1.217(3)	0.004
(9-fluorenone)($AlCl_3$)·C_7H_8 (neutral fluorenone)[28]			1.756(3)		1.283(4)	0.006
(9-fluorenone)($GaCl_3$)·C_7H_8 (neutral fluorenone)[28]			1.916(5)		1.259(4)	0.136
{(Fl=O$^{\bullet-}$)(Na^+)($C_6H_{18}N_3PO$)}$_4$ (fluorenone ketyl radical anion)[29]			2.314(5) Na^I-O		1.272(5)	0.135
$C_{51}H_{70}O_5Sm$·C_6H_6 (fluorenone ketyl radical anion)[30]			2.159(5) Sm^{III}-O		1.313(5)	0.010
$C_{62}H_{56}AlN_2O_2$·CH_2Cl_2 (fluorenone ketyl dimer)[23]			1.748(5) Al^{III}-O 1.744(5) Al^{III}-O		1.412(5) 1.419(5)	0.774 0.766
$C_{34}H_{36}Cl_4N_2O_2V_2$ (fluoren-9-olato$^-$ anion)[31]			1.807(4) V^V-O		1.4454)	0.785
$C_{40}H_{37}AlN_4O_2$·CH_2Cl_2 (fluoren-9-olato$^-$ anion)[32]			1.743(4) Al^{III}-O		1.411(5)	1.021

d. Magnetic properties.

Magnetic properties of **1**-**3** were studied by SQUID and EPR techniques. The salts show effective magnetic moments of 1.72, 1.66 and 1.79 μ_B at 300 K (Figs. 5a, S4a and S5a, respectively) due to the presence of unpaired spins on the $Pc^{\bullet 3-}$ macrocycle, whereas the HFl-O^- anions are diamagnetic and do not contribute to magnetic susceptibility of **1** and **2**. Weiss temperatures estimated in the 40-300 K range of -22, -14 and -30 K (Figs. 5b, S4b and S5b, respectively) show antiferromagnetic coupling of spins while no magnetic ordering is observed down to 1.9 K. Magnetic moments are constant at high temperatures but decrease with temperature approximately below 200 K most probably due to antiferromagnetic coupling of spins. Fitting of the experimental data for **1** and **2** by the Heisenberg model for antiferromagnetic coupling of spins in the two-dimensional square layers[34] was made with exchange interaction of $J/k_B = -1.1$ (1) and -0.9 K, respectively (Figs. S7 and S8, respectively). The relatively weak magnetic coupling is most probably realized in the two-dimensional corrugated phthalocyanine layers since phthalocyanines form distorted but nearly square arrangement with side-by-side van der Waals C···C contacts between $Pc^{\bullet 3-}$ parallel to the *ab*-plane (Fig. 3b). Experimental data for **3** can be fitted in the 12-300 K range by the Heisenberg model for pairs of antiferromagnetically coupling spins[35] with exchange interaction of J/k_B = -10.8 K (Fig. S9). This magnetic coupling is most probably realized within isolated π-stacking $\{[In^{III}Br(Pc^{\bullet 3-})]^{\bullet -}\}_2$ dimers (Fig. 4b). It should be noted that in case of **3** intradimer magnetic coupling is essentially stronger than those in salts **1** and **2** but less effective than those observed for previously studied $\{[Ti^{IV}O(Pc^{\bullet 3-})]^{\bullet -}\}_2$ [6] and $\{Ph_5CpRu(CO)_2[Sn^{II}(Pc^{\bullet 3-})]^{\bullet -}\}_2$ dimers[8].

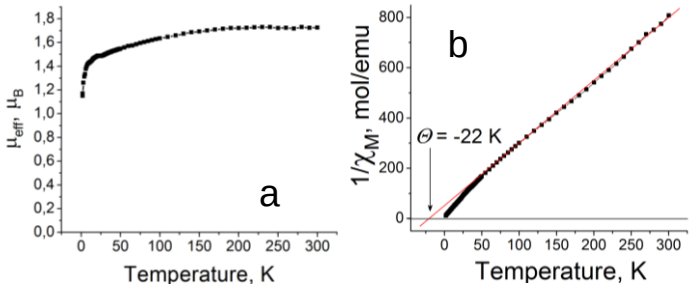

Fig. 5. Temperature dependences of effective magnetic moments for polycrystalline **1** (a); temperature dependences of reciprocal magnetic susceptibility for polycrystalline **1** (b).

Salt **1** shows an intense narrow Lorentzian EPR signal with g = 1.9987 and the linewidth (ΔH) of 0.474 mT at 298 K for **1** (Fig. 6a). Obviously this signal can be attributed to $Pc^{\bullet 3-}$. Comparing to this, the $H_2Pc^{\bullet -}$ radical anion shows a slightly narrower EPR signal with ΔH = 0.1-0.2 mT.[6, 36] The signal

exhibits nearly temperature independent *g*-factor and ΔH down to down to 100 K and is split into two lines below this temperature (Fig. 6b). Both lines are noticeably broadened below 50 K and their *g*-factors shift into opposite directions (Figs. 6c and 6d). These lines have g_1 = 2.0007 and ΔH = 0.525 mT and g_2 = 1.9946 and ΔH = 1.217 mT at 4.2 K. The observed broadening and *g*-factor shift can be attributed to the antiferromagnetic coupling of spins observed in **1** in the phthalocyanine layers.

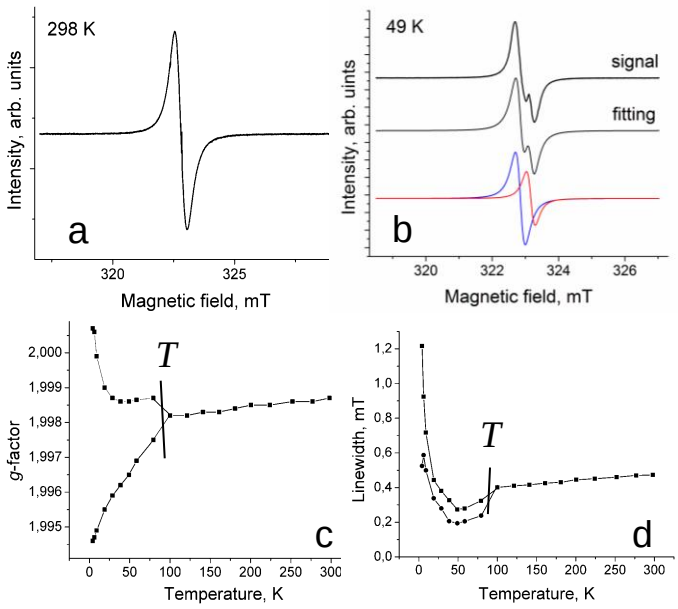

Fig. 6. The EPR signal of polycrystalline **1** at 298 (a) and 49 K (b). In (b), the fitting of the signal by two Lorentzian lines is shown in middle and bottom; temperature dependence of *g*-factor (c) and linewidth (d) of the EPR signal of polycrystalline **1**. The EPR signal splitting temperature into two lines is marked as *T*).

Salt **2** has crystal structure similar to that of **1** but weaker antiferromagnetic coupling of spins in the phthalocyanine layers. It shows an essentially broader EPR signal which can be approximated by two Lorentzian lines. The main line has g_1 = 1.9988 and ΔH = 3.27 mT at 293 K (Fig. S6a). The narrower line with g_2 = 2.0012 and ΔH = 1.02 mT at 293 K has essentially smaller intensity which is only few percent of that of the broad signal. The *g*-factor of narrower signal is nearly temperature independent (Fig. S6c), and becomes slightly narrower with temperature decrease down to 4.2 K (Fig. S6d). The narrower line can originate from impurities. The main broad line strongly narrows with the temperature decrease (Fig. S6d). Below 170 K this line splits in two lines, and three lines are observed below 70 K. Such behavior shows signal anisotropy at low temperatures. As a result, the EPR signal contains four

lines below 70 K (Fig. S6b). In contrast to **1**, no essential broadening of the EPR signal is observed for **2** at low temperatures.

In contrast to **1** and **2**, salt **3** has an asymmetric signal even at room temperature with g_1 = 1.9857 (ΔH = 14.18 mT) and g_2 = 1.9968 (ΔH = 9.68 mT) (Fig. 7a, 295 K). Both lines have nearly equal integral intensities and are very broad in comparison with those of **1** and **2**. One of the lines is spilt into two lines below 80 K, and totally three lines appear below this temperature (Figs. 7b-d) showing anisotropy of the EPR signal from **3**. All three lines are slightly broadened below 50 K most probably also due to antiferromagnetic coupling of spins within the dimers.

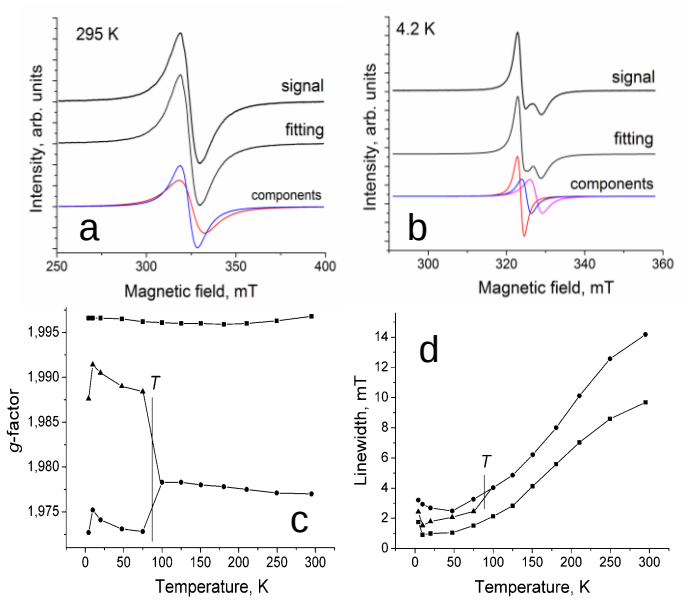

Fig. 7. EPR signal of polycrystalline **3** at 295 (a) and 4.2 K (b). In (b), the fitting of the signals by two Lorentzian lines is shown in middle and bottom; Temperature dependence of *g*-factor (c) and linewidth (d) of EPR signal of polycrystalline **3**. Temperature of EPR line splitting into two lines is marked as *T*.

It is seen from the analysis of the EPR data for salts **1-3** that in all cases EPR signals are anisotropic and split into 2-3 lines at low temperatures. It was found that the size of central metal atom affects strongly the width of EPR signals from $Pc^{\bullet 3-}$ (the maximal width is attained for the EPR signal of **3** (In^{III}) and the minimal width is attained for the EPR signal of **1** (Al^{III})). The signals have *g*-factors smaller than 2.0000 and the smallest *g*-factor values were found for **3** (In^{III}). Antiferromagnetic coupling of spins is regarded to result in the broadening of EPR lines which is most effectively takes place in **1** below 50 K, while absent in **2** and only weakly works in **3** below 50 K. Previously EPR spectra of neutral radicals $[Al^{III}(MeIm)_2(Pc^{\bullet 3-})]^{\bullet}\cdot MeIm$ and $[Ga^{III}(MeIm)_2(Pc^{\bullet 3-})]^{\bullet}\cdot 2C_6H_4Cl_2$ also

containing $Pc^{\bullet 3-}$ were analyzed. In these cases both signals were rather narrow with ΔH = 0.55-0.65 mT and *g*-factor was in the 2.00011- 2.0028 range.[10]

e. Theoretical analysis

In order to clarify molecular and spin structures theoretically, the full geometry optimization in the doublet state of $[Al^{III}(HFl–O^{-})(Pc^{\bullet 3-})]^{\bullet -}$, and the singlet and triplet states of $[Al(Fl{=}O^{\bullet -})(Pc^{\bullet 3-})]^{2\bullet -}$ were performed at the UM11/6-31+G(d,p) level of theory, where the X-ray structure of **1** was used as initial structure. Total and relative energies, number of imaginary frequency, $\langle S^2 \rangle$ values, and charge and spin densities are summarized in Tables S2 and S3.

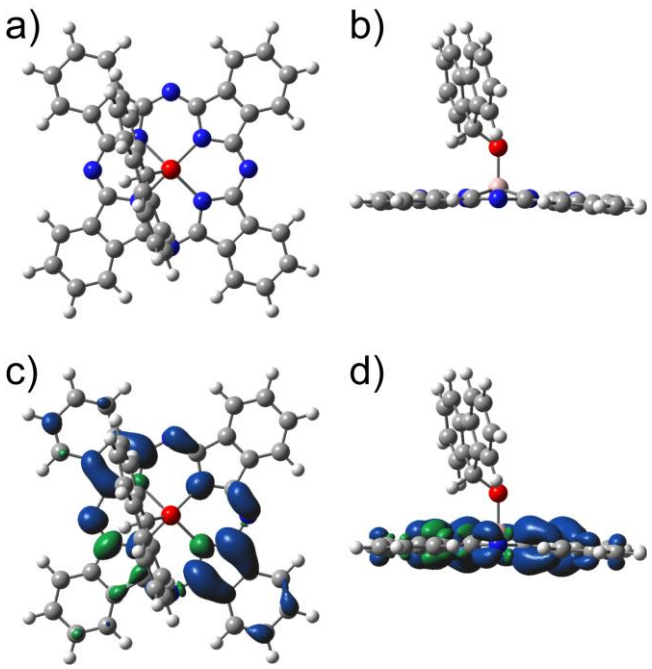

Fig. 8. (a) Top and (b) side views of optimized structure in the ^2A state of $[Al(HFl–O^{-})(Pc^{\bullet 3-})]^{\bullet -}$ at the UM11/6-31+G(d,p) level of theory. (c) Top and (d) side views of the spin density distribution, where the isosurface value is 0.0016 electron/au^3. The isosurfaces in blue and green denote the positive and negative spin density, respectively

The optimized structures in the ^2A state of $[Al(HFl–O^{-})(Pc^{\bullet 3-})]^{\bullet -}$ and the ^1A state of $[Al(Fl{=}O^{\bullet -})(Pc^{\bullet 3-})]^{2\bullet -}$ are shown in Figs. 8 and S10. The oxygen atom obviously shows the out-of-plane deviation from the fluorene plane in the optimized structure of $[Al(HFl–O^{-})(Pc^{\bullet 3-})]^{\bullet -}$ (Fig. 8), whereas oxygen atom lies on the fluorene plane in $[Al(Fl{=}O^{\bullet -})(Pc^{\bullet 3-})]^{2\bullet -}$ (Fig. S10). Spin density of almost unity localizes on the Pc ligand in $[Al(HFl–O^{-})(Pc^{\bullet 3-})]^{\bullet -}$, indicating that the magnetic property stems from

the π-radical spin on the $Pc^{\bullet 3-}$ radical anion (Figs. 8c and 8d, Table S3). However, two moieties of Pc ligand and fluorenone show the radical character in $[Al(Fl{=}O^{\bullet -})(Pc^{\bullet 3-})]^{2\bullet -}$ (Fig. S10 and Table S3). Therefore, it is obvious that the experimental results support the existence of $[Al(HFl{-}O^{-})(Pc^{\bullet 3-})]^{\bullet -}$ in **1** rather than $[Al(Fl{=}O^{\bullet -})(Pc^{\bullet 3-})]^{2\bullet -}$.

Conclusion

Tetrabutylammonium salts of aluminum(III), gallium(III) and indium(III) phthalocyanine chlorides were obtained as single crystals. In contrast to previously studied phthalocyanines of Ni^{II}, Cu^{II}, Sn^{II}, Pb^{II}, H_2, Fe^{II}, $Ti^{IV}O$ and $V^{IV}O$, aluminum(III) and gallium(III) strongly tend to be coordinated by oxygen containing fluoren-9-olato$^-$ anion which is most probably formed by hydrogen abstraction from solvent by fluorenone ketyl reductant. Al^{III}ClPc and Ga^{III}ClPc in the reduced form show catalytic activity in conversion of *o*-dichlorobenzene to *p*-dichlorobenzene. Indium(III) phthalocyanine does not coordinate to the HFl-O^- anion. Instead of that a bromide anion from Bu_4NBr substitutes a chloride anion at indium(III) atoms. Reduction of these metal phthalocyanines is accompanied by the formation of $Pc^{\bullet 3-}$ providing strong blue shift of the Q and Soret bands of Pc, the appearance of new NIR bands at 1007-1013 nm, and partial disruption of aromaticity of the Pc macrocycle evidenced for **3**. The $Pc^{\bullet 3-}$ species have S = 1/2 spin state in **1**-**3** and spins of the macrocycles are antiferromagnetically coupled in two-dimentional layers of **1** and **2** and π-stacking dimers of **3**. EPR signals of **1**-**3** show obvious tendency to broadening with increasing size of central metal atom, the anisotropy especially at low temperature, and relatively small g-factor values (< 2.000) in comparison with those of other metal phthalocyanine radical anion salts[6].

Experimental Section

Materials. Al^{III}ClPc (>85% purity), Ga^{III}ClPc (>97% purity) and In^{III}ClPc (>98% purity) were purchased from Aldrich and were used without further purification. Tetrabutylammonium bromide $(Bu_4N^+)(Br^-)$ of 99% purity was purchased from TCI. Sodium fluorenone ketyl was obtained as previously described[37]. All manipulations for the syntheses of **1** - **3** were carried out in a MBraun 150B-G glove box with controlled atmosphere and the content of H_2O and O_2 less than 1 ppm. Solvents were purified in argon atmosphere. *o*-Dichlorobenzene ($C_6H_4Cl_2$) was distilled over CaH_2 under reduced pressure and hexane was distilled over Na/benzophenone. The crystals of **1** - **3** were stored in a glove box. KBr pellets for IR- and UV-visible-NIR measurements were also prepared in a glove box. EPR and SQUID magnetic measurements were performed on weighed polycrystalline samples of **1** - **3** sealed in 2 mm quarz tubes under 10^{-5} Torr.

General. UV-visible-NIR spectra were measured in KBr pellets on a Perkin Elmer Lambda 1050 spectrometer in the 250-2500 nm range. FT-IR spectra were obtained in KBr pellets with a Perkin-Elmer Spectrum 400 spectrometer (400-7800 cm^{-1}). EPR spectra were recorded for polycrystalline samples of **1** and **2** with a JEOL JES-TE 200 X-band ESR spectrometer equipped with a JEOL ES-CT470 cryostat working between room and liquid helium temperatures. A Quantum Design MPMS-XL SQUID magnetometer was used to measure static magnetic susceptibility of **1** - **3** at 100 mT magnetic field in cooling and heating conditions in the 300 − 1.9 K range. A sample holder contribution and core temperature independent diamagnetic susceptibility (χ_d) were subtracted from the experimental values. The χ_d values were estimated by the extrapolation of the data in the high-temperature range by fitting the data with the following expression: $\chi_M = C/(T - \Theta) + \chi_d$, where C is Curie constant and Θ is Weiss temperature. Effective magnetic moment (μ_{eff}) was calculated with the following formula: $\mu_{eff} = (8 \cdot \chi_M \cdot T)^{1/2}$.

Synthesis. Crystals of **1** - **3** were obtained by diffusion technique. A reaction mixture was filtered into a 1.8-cm diameter, 50 mL glass tube with a ground glass plug, and then 30 mL of hexane was layered over the solution. Slow mixing of two solvents resulted in precipitation of crystals over 1 month. The solvent was then decanted from the crystals, and they were washed with hexane. The composition of the obtained salts was determined from X-ray diffraction analysis on a single crystal. Several crystals from one synthesis were found to consist of a single crystalline phase. Because of high air sensitivity of **1** - **3**, elemental analysis could not be used to determine the composition since the salts reacted with oxygen in the air before the quantitative oxidation procedure could be performed.

The crystals of $(Bu_4N)_2\{M^{III}(HFl–O)Pc\}(Br)\cdot 1.5C_6H_4Cl_2$ (M = Al (**1**), Ga (**2**)) and $(Bu_4N)[In^{III}BrPc]\cdot 0.875C_6H_4Cl_2\cdot 0.125C_6H_{14}$ (**3**) were obtained by the following procedure. $Al^{III}ClPc$ (24 mg, 0.042 mmol for **1**) or $Ga^{III}ClPc$ (25.8 mg, 0.042 mmol for **2**) or $In^{III}ClPc$ (26.4 mg, 0.042 mmol for **3**) in 16 ml of $C_6H_4Cl_2$ was reduced by a triple excess of sodium fluorenone ketyl (26 mg, 0.128 mmol) in the presence of an excess of $(Bu_4N^+)(Br^–)$ (50 mg, 0.155 mmol) during 4 hours at 120°C to yield deep blue-violet solution. The solution was cooled down to room temperature and filtered into the tube for diffusion. Crystals of black color with characteristic copper luster were obtained as elongated plates and prisms for **1** and **2** (the yields are 52 and 44%, respectively) and as prisms for **3** (the yield is 62%).

X-ray crystal structure determination. Crystal data of **1** at 150(2) K: $C_{86}H_{102}AlBrCl_3N_{10}O$, M_r = 1506.02 g mol^{-1}, black elongated plate, monoclinic, $P\ 2_1/c$, a = 12.8652(6), b = 22.7732(10), c = 27.5698(12) Å, β = 99.82(3)°, V = 7959.1(6) $Å^3$, Z = 4, d_{calc} = 1.257 g·cm^{-3}, μ = 0.681 mm^{-1}, F(000) =

3184, $2\theta_{max}$ = 51.62°, reflections measured 82270, unique reflections 15300, reflections with $I > 2\sigma(I)$ = 11822, parameters refined 927, restraints 0, R_1 = 0.0628, wR_2 = 0.1857, G.O.F. = 1.051, CCDC 1530033.

Crystal data of **2** at 150(2) K: $C_{86}H_{102}GaBrCl_3N_{10}O$, M_r = 1548.76 g mol^{-1}, black prism, monoclinic, $P\ 2_1/c$, a = 12.6360(11), b = 22.7281(18), c = 27.756(3) Å, β = 100.054(10) °, V = 7848.9(13) Å^3, Z = 4, d_{calc} = 1.311 g·cm^{-3}, μ = 1.015 mm^{-1}, $F(000)$ = 3256, $2\theta_{max}$ = 52.816°, reflections measured 71938, unique reflections 16111, reflections with $I > 2\sigma(I)$ = 11001, parameters refined 932, restraints 316, R_1 = 0.1387, wR_2 = 0.3043, G.O.F. = 1.172, CCDC 1530009.

Crystal data of **3** at 85(1) K: $C_{108}H_{114.50}Br_2Cl_{3.50}In_2N_{18}$, M_r = 2178.20 g mol^{-1}, black prism, triclinic, $P\ \bar{1}$, a = 13.8496(2), b = 17.0611(3), c = 21.3800(3) Å, α = 90.084(1), β = 91.958(1), γ = 98.5090(10)°, V = 4993.23(13) Å^3, Z = 2, d_{calc} = 1.449 g·cm^{-3}, μ = 1.414 mm^{-1}, $F(000)$ = 2232, $2\theta_{max}$ = 56.562°, reflections measured 61175, unique reflections 24257, reflections with $I > 2\sigma(I)$ = 19857, parameters refined 1314, restraints 537, R_1 = 0.0635, wR_2 = 0.1823, G.O.F. = 1.044, CCDC 1530033.

X-ray diffraction data for the crystals of **1** and **3** were collected on a Bruker Smart Apex II CCD diffractometer with graphite monochromated MoK$_\alpha$ radiation using a Japan Thermal Engineering Co. cooling system DX-CS190LD. Raw data reduction to F^2 was carried out using Bruker SAINT.[38] X-ray diffraction data for **2** were collected on an Oxford diffraction "Gemini-R" CCD diffractometer with graphite monochromated MoK$_\alpha$ radiation using an Oxford Instrument Cryojet system. Raw data reduction to F^2 was carried out using CrysAlisPro, Oxford Diffraction Ltd. The structures were solved by direct method and refined by the full-matrix least-squares method against F^2 using SHELX 2013 and 2014.[39] Non-hydrogen atoms were refined in the anisotropic approximation. Positions of hydrogen were calculated geometrically. One of two positions of solvent molecules is shared by both *o*-$C_6H_4Cl_2$ and *p*-$C_6H_4Cl_2$ solvent molecules in the 0.356(4)/0.144(4) ratio. In contrast to **1** salt **2** most probably slowly losses solvent molecules and this process increases the disorder of the components in **2**. As a result in contrast to **1** bromine anions are disordered between three positions in **2** with the occupancies of 0.429(3), 0.493(3) and 0.078(3) (total occupancy is 1). Structure of **3** also contains disordered components. One of two TBA^+ cations is disordered between two orientation with the occupancies of 0.864(8) and 0.136(8). Solvent $C_6H_4Cl_2$ and C_6H_{14} molecules are also disordered and share several positions in the 0.875(4)/0.125(4) ratio. To keep the anisotropic thermal parameters of the disordered atoms within reasonable limits the displacement components were restrained using ISOR, SIMU and DELU SHELXL instructions. That resulted in 316 and 537 restraints used for the refinement of the crystal structures of **2** and **3**, respectively.

Computational detail. DFT calculations based on the M11 functional[40] were performed using the 6-31+G(d,p) basis set. For the full geometry optimization, “Opt = Tight” was specified, and frequency

calculations confirmed no imaginary frequency. In the present DFT calculations, “Int =SuperFineGrid” was specified, and the stabilities of the wave functions were confirmed by specifying the “Stable = Opt” keyword. The subsequent natural bond orbital (NBO) analysis was performed using the NBO program.[41] The computations were performed with the Gaussian 09 program package.[42]

Acknowledgements

The work was supported by RSF grant № 17-13-01215, and by JSPS KAKENHI Grant Numbers 15K17901, 23225005, and 26288035. Theoretical calculations were performed at the Super Computer System, Institute for Chemical Research, Kyoto University, and under Collaborative Research Program for Young Scientists at Academic Center for Computing and Media Studies, Kyoto University.

Keywords: aluminum, gallium and indium phthalocyanines, radical anion salts of metal phthalocyanines, crystal structure, optical and magnetic properties, antiferromagnetic coupling

[1] J. L. Petersen, C. S. Schramm, D. R. Stojakovic, B. M. Hoffman, T. J. Marks, *J. Am. Chem. Soc*. **1977**, *99*, 286–288.

[2] H. Hasegawa, T. Naito, T. Inabe, T. Akutagawa, T. Nakamura, *J. Mater. Chem*. **1998**, *8*, 1567–1570.

[3] T. Inabe, H. Tajima, *Chem. Rev*. **2004**, *104*, 5503–5534.

[4] J. S. Miller, C. Vazquez, J. C. Calabrese M. L. McLean, A. J. Epstein, *Adv. Mater*. **1994**, *6*, 217-221.

[5] D. K. Rittenberg, L. Baars-Hibbe, A.B. Böhm, J.S. Miller, *J. Mater. Chem*. **2000**, *10*, 241–244.

[6] D. V. Konarev, A. V. Kuzmin, M. A. Faraonov, M. Ishikawa, Y. Nakano, S. S. Khasanov, A. Otsuka, H. Yamochi, G. Saito, R. N. Lyubovskaya, *Chem. Eur. J*. **2015**, *21*, 1014–1028.

[7] D. V. Konarev, S. I. Troyanov, M. Ishikawa, M. Faraonov, A. Otsuka, H. Yamochi, G. Saito, R. N. Lyubovskaya, *J. Porph. Phth*. **2014**, *18*, 1157–1163.

[8] D. V. Konarev, A. V. Kuzmin, Y. Nakano, M. A. Faraonov, S. S. Khasanov, A. Otsuka, H. Yamochi, G. Saito, R. N. Lyubovskaya, *Inorg. Chem.* **2016**, *55*, 1390–1402.

[9] E. W. Y. Wong, D. B. Leznoff, *J. Porph. Phth.* **2012**, *16*, 154–162.

[10] D. V. Konarev, A. V. Kuzmin, S. S. Khasanov, A. Otsuka, H. Yamochi, G. Saito, R. N. Lyubovskaya, *Eur. J. Inorg. Chem.* **2016**, 4099-4103.

[11] J. A. Cissell, T. P. Vaid, A. L. Rheingold, *Inorg. Chem.* **2006**, *45*, 2367–2369.

[12] D. V. Konarev, A. V. Kuzmin, S. S. Khasanov, M. Ishikawa, A. Otsuka, H. Yamochi, G. Saito, R. N. Lyubovskaya, *Dalton Trans*. **2016**, *45*, 10780 - 10788.

[13] J. A. Cissell, T. P. Vaid, A. G. DiPasquale, A. L. Rheingold, *Inorg. Chem*. **2007**, *46*, 7713–7715.

[14] E. W. Y. Wong, C. J. Walsby, T. Storr, D. B. Leznoff, *Inorg. Chem*. **2010**, *49*, 3343–3350.

[15] M. Tahiri, P. Doppelt, J. Fischer, R. Weiss, *Inorg. Chim. Acta* **1987**, *127*, L1–L3.

[16] H. Huckstadt, H. Homborg, *Z. Anorg. Allg. Chem.* **1998**, *624*, 715–720.

[17] D. V. Konarev, S. S. Khasanov, M. Ishikawa, A. Otsuka, H. Yamochi, G. Saito, R. N. Lyubovskaya, *Inorg. Chem*. **2013**, *52*, 3851–3859.

[18] D. V. Konarev, A. V. Kuzmin, S. S. Khasanov, R. N. Lyubovskaya, *Dalton Trans*. **2013**, *42*, 9870–9876.

[19] D. V. Konarev, L. V. Zorina, M. Ishikawa, S. S. Khasanov, A. Otsuka, H. Yamochi, G. Saito, R. N. Lyubovskaya, *Cryst. Groth Des*. **2013**, *13*, 4930−4939.

[20] D. V. Konarev, A. V. Kuzmin, M. Ishikawa, Y. Nakano, M. A. Faraonov, S. S. Khasanov, A. Otsuka, H. Yamochi, G. Saito, R. N. Lyubovskaya, *Eur. J. Inorg. Chem.* **2014**, 3863– 3870.

[21] E. Tosatti, M. Fabrizio, J. Tóbik, G. E. Santoro, *Phys. Rev. Lett*. **2004**, *93*, 117002.

[22] D. V. Konarev, L. V. Zorina, S. S. Khasanov, E. U. Hakimova, R. N. Lyubovskaya, *New J. Chem.* **2012**, *36*, 48–51.

[23] D. V. Konarev, S. I. Troyanov, R. N. Lyubovskaya, *CrystEngComm*., **2015**, *17*, 3923-3936,

[24] I. L. Fedushkin, A. N. Lukoyanov, G. K. Fukin, M. Hummert, H. Schumann, *Russ. Chem. Bull.* **2006**, *55*, 1177-1183.

[25] D. V. Konarev, A. V. Kuzmin, S. S. Khasanov, A. Otsuka, H. Yamochi, G. Saito, R. N. Lyubovskaya, *Dalton Trans*. **2014**, *43*, 13061-13069.

[26] G. A. Olah, W. S. Tolgyesi, R. E. A. Dear, J. Org. Chem., 1962, 27, 3449-3455.

[27] H. R. Luss, D. L. Smith, *Acta Crystallogr., Sect. B: Struct. Crystallogr. Cryst. Chem.* **1972**, *28*, 884-889.

[28] C. S. Branch, S. G. Bott, A. R. Barron, *J. Organomet. Chem.* **2003**, *666*, 23-34.

[29] Z. Hou, X. Jia, A. Fujita, H. Tezuka, H. Yamazaki, Y. Wakatsuki, *Chem. Eur. J.* **2000**, *6*, 2994-3005.

[30] Z. Hou, A. Fujita, Y. Zhang, T. Miyano, H. Yamazaki, Y. Wakatsuki, *J. Am. Chem. Soc.* **1998**, *120*, 754-766.

[31] F. Preuss, U. Fischbeck, F. Tabellion, J. Perner, W. Frank, G. Reiss, *Z. Naturforsch., B: Chem. Sci.* **2001**, *56*, 255-262.

[32] C.-Y. Lin, C.-F. Tsai, H.-J. Chen, C.-H. Hung, R.-C. Yu, P.-C. Kuo, H. M. Lee, J.-H. Huang, *Chem. Eur. J.* **2006**, *12*, 3067-3073.

[33] K. Yamasaki, O. Okada, K. Inami, K. Oka, M. Kotani, H. Yamada, *J. Phys. Chem. B*, **1997**, *101*, 13-19.

[34] M. E. Lines, *J. Phys. Chem. Solids* **1970**, *31*, 101–l16.

[35] J. S. Smart, In Magnetism III, Eds. G. T. Rado, H. Suhl, Academic Press, NY, **1963**, p. 63.

[36] D. V. Konarev, L. V. Zorina, S. S. Khasanov, A. L. Litvinov, A. Otsuka, H. Yamochi, G. Saito, R. N. Lyubovskaya, *Dalton Trans.* **2013**, *42*, 6810-6816.

[37] D. V. Konarev, S. S. Khasanov, E. I. Yudanova, R. N. Lyubovskaya, *Eur. J. Inorg. Chem.* **2011**, 816-820.

[38] Bruker Analytical X-ray Systems, Madison, Wisconsin, U.S.A, **1999**.

[39] G. M. Sheldrick, *Acta Cryst. Sec. A* **2008**, *64*, 112-122.

[40] R. Peverati, D. G. Truhlar, *J. Phys. Chem. Lett.* **2011**, *2*, 2810-2817.

[41] NBO Version 3.1, E. D. Glendening, A. E. Reed, J. E. Carpenter, F. Weinhold.

[42] Gaussian 09, Revision D.01, M. J. Frisch, G. W. Trucks, H. B. Schlegel, G. E. Scuseria, M. A. Robb, J. R. Cheeseman, G. Scalmani, V. Barone, B. Mennucci, G. A. Petersson, H. Nakatsuji, M. Caricato, X. Li, H. P. Hratchian, A. F. Izmaylov, J. Bloino, G. Zheng, J. L. Sonnenberg, M. Hada, M. Ehara, K. Toyota, R. Fukuda, J. Hasegawa, M. Ishida, T. Nakajima, Y. Honda, O. Kitao, H. Nakai, T. Vreven, J. A. Montgomery, Jr., J. E. Peralta, F. Ogliaro, M. Bearpark, J. J. Heyd, E. Brothers, K. N. Kudin, V. N. Staroverov, T. Keith, R. Kobayashi, J. Normand, K. Raghavachari, A. Rendell, J. C. Burant, S. S. Iyengar, J. Tomasi, M. Cossi, N. Rega, J. M. Millam, M. Klene, J. E. Knox, J. B. Cross, V. Bakken, C. Adamo, J. Jaramillo, R. Gomperts, R. E. Stratmann, O. Yazyev, A. J. Austin, R. Cammi, C. Pomelli, J. W. Ochterski, R. L. Martin, K. Morokuma, V. G. Zakrzewski, G. A. Voth, P. Salvador, J. J. Dannenberg, S. Dapprich, A. D. Daniels, O. Farkas, J. B. Foresman, J. V. Ortiz, J. Cioslowski, and D. J. Fox, Gaussian, Inc., Wallingford CT, 2013.

Table of Contents

FULL PAPER

Crystalline salts $(Bu_4N^+)_2[M^{III}(HFl\text{-}O^-)(Pc^{\bullet 3-})]^{\bullet -}(Br^-)\cdot 1.5C_6H_4Cl_2$ (M = Al (**1**), Ga (**2**)) containing aluminum(III) and gallium(III) phthalocyanine radical anions and diamagnetic fluoren-9-olato$^-$ anions (HFl-O$^-$) coordinated to metal(III) centers and $(Bu_4N^+)[In^{III}Br(Pc^{\bullet 3-})]^{\bullet -}\cdot$Solvent (**3**) with indium(III) bromide phthalocyanine radical anions have been obtained. Their syntheses, crystal structures, optical and magnetic properties are discussed.

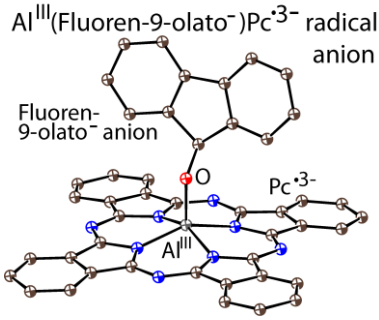

D. V. Konarev, S.S. Khasanov, M. Ishikawa, Y. Nakano, A. Otsuka, H. Yamochi, G. Saito and R. N. Lyubovskaya*

Page No. – Page No.

Tetrabutylammonium salts of aluminum(III) and gallium(III) phthalocyanine radical anions bonded with fluoren-9-olato$^-$ anions and indium(III) bromide phthalocyanine radical anions

Supporting information.

Table S1. IR spectra of the starting compounds and salts **1 - 3**

Components	$(TBA^+)(Br^-)$	$(Na^+)(Fl{=}O^{\bullet-})$	$Al^{III}ClPc^{2-}$	$(TBA^+)_2[Al^{III}(HFl\text{-}O^-)(Pc^{\bullet3-})]^{\bullet-}(Br^-)\cdot1.5C_6H_2Cl_2$ (**1**)	$Ga^{III}ClPc^{2-}$	$(TBA^+)_2[Ga^{III}(HFl\text{-}O^-)(Pc^{\bullet3-})]^{\bullet-}(Br^-)\cdot1.5C_6H_2Cl_2$ (**2**)	$In^{III}ClPc^{2-}$	$(TBA^+)[In^{III}Br(Pc^{\bullet3-})]^{\bullet-}\cdot0.875C_6H_4Cl_2\cdot0.125C_6H_{14}$ (**3**)
$M^{III}Pc$			433w	438w	430w	439w	438w	437w
			516w	516w	507w	503w	498w	492w
			574w	572w	572w	570w	635w	634w
			728s	725s*	733s	715s*	724s	711s
			762m	755s*	755m	752s*	749m	748s*
			-	-	780m	766w	771m	767m
			904w	900w*	897m	897s*	885m	880w*
			1064s	1066w*	1062s	1060w*	1059m	-
			-	-	-	-	1084s	1091m*
			1120m	1120s*	1121s	1110s*	1118s	1114s*
			1136m	-	-	-	-	-
			1165w	1167w*	1169m	1166w*	-	-
			1288m	1295m*	1288m	1290w*	1285m	1287m
			1332s	1328m	1332s	1323w	1332s	1324m
			1425w	1423m	1423m	1421w	-	1417s
			1464w	1471m*	1467w	1464s*	-	-
			-	-	1484w	1475s*	1473m	1481m*
			1502m	-	1506m	-	-	-
			1609w	1603w	1608w	1601w	1610w	-
			3049w	3060w*	3050w	3036w	3045w	3049w
TBA^+	738s			738s*		738m*		748s*
	883s			880w		884m		880w*
	896s			900w*		897s*		-
	922s			-		923m*		-
	992s			1002w		993w		999w
	1031m			1033w*		1031w*		1032w*
	1059m			-		1060w*		-
	1069m			1066w*		1070w		-
	1110s			1120s*		1110s*		1114s*
	1166s			1167w		1166w*		1167m
	1240m			-		1240w		1263w
	1365m			-		1366w		-
	1379m			1379m		1380m		1380w
	1455s			1456s*		1454s*		1455s*
	1464s			-		1464s*		-
	1474s			1471m*		1475s*		1481m*
	2873w			2872w		2873w		2871w
	2959w			2959w		2960w		2960w
Fluorenone-anions		722s		725s*		715s*		
		734s		738s*		738m*		
		756m		755s*		752s*		
		922m		-		923m*		
		1197m		1196w		-		
		1302m		1295m*		-		
		1393s		-		1399w		
		1400s		-		1408w		
		1440s		-		-		
		1452s		1456s*		1454s*		
		1491s		-		1475s		
		1593s		1571w		-		
		1609m		-		1601w		
		1674m		-		-		
		3049w		3060w*		3036w		
$C_6H_4Cl_2$				658w		-		658w
				755s*		752s*		748s*
				1033w*		1031w*		1032w*
				1456s*		1454s*		1455s*

w – weak, m-middle, s – strong intensity; * - the bands are coincided.

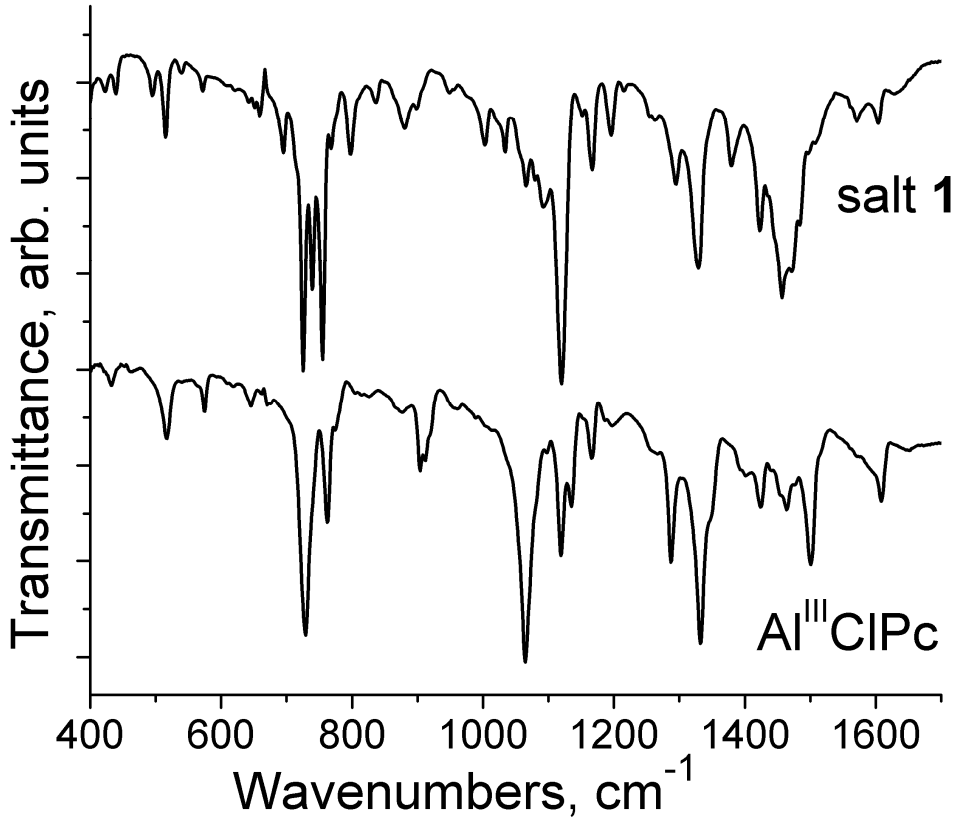

Fig. S1. IR spectrum of starting $Al^{III}Cl(Pc^{2-})$ and salt **1** in KBr pellets. KBr pellet for **1** was prepared in the glove box.

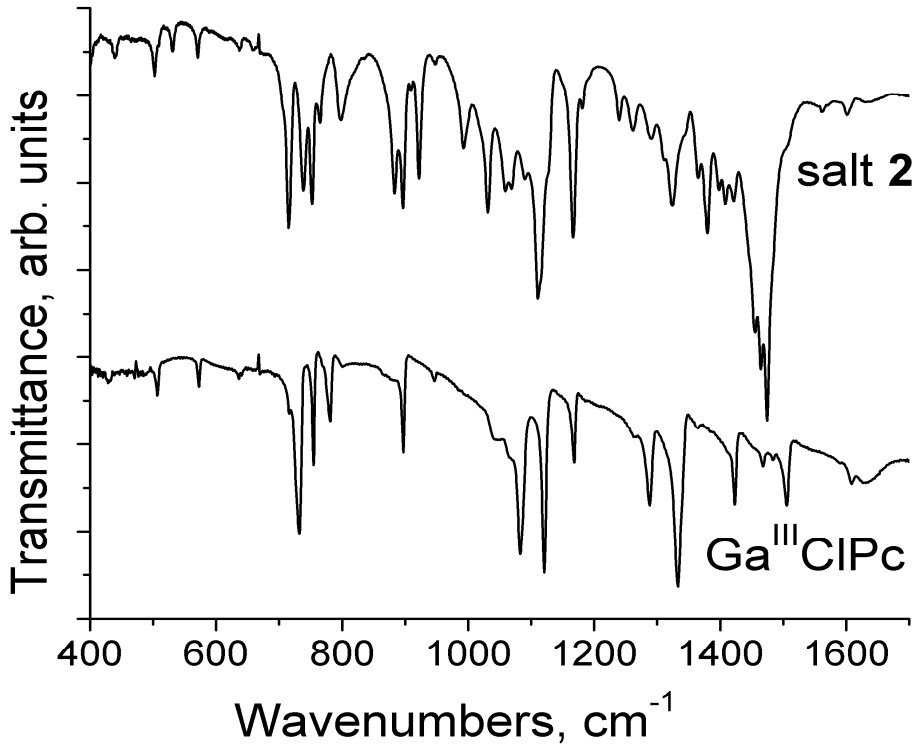

Fig. S2. IR spectrum of starting $Ga^{III}Cl(Pc^{2-})$ and salt **2** in KBr pellets. KBr pellet for **2** was prepared in the glove box.

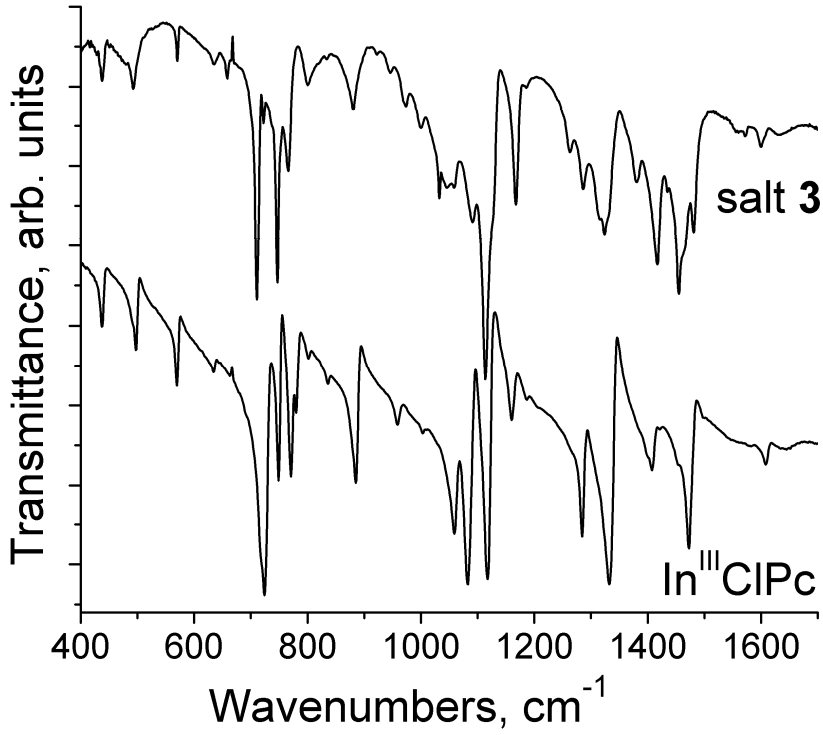

Fig. S3. IR spectrum of starting $In^{III}Cl(Pc^{2-})$ and salt **3** in KBr pellets. KBr pellet for **3** was prepared in the glove box.

Data of magnetic measurements.

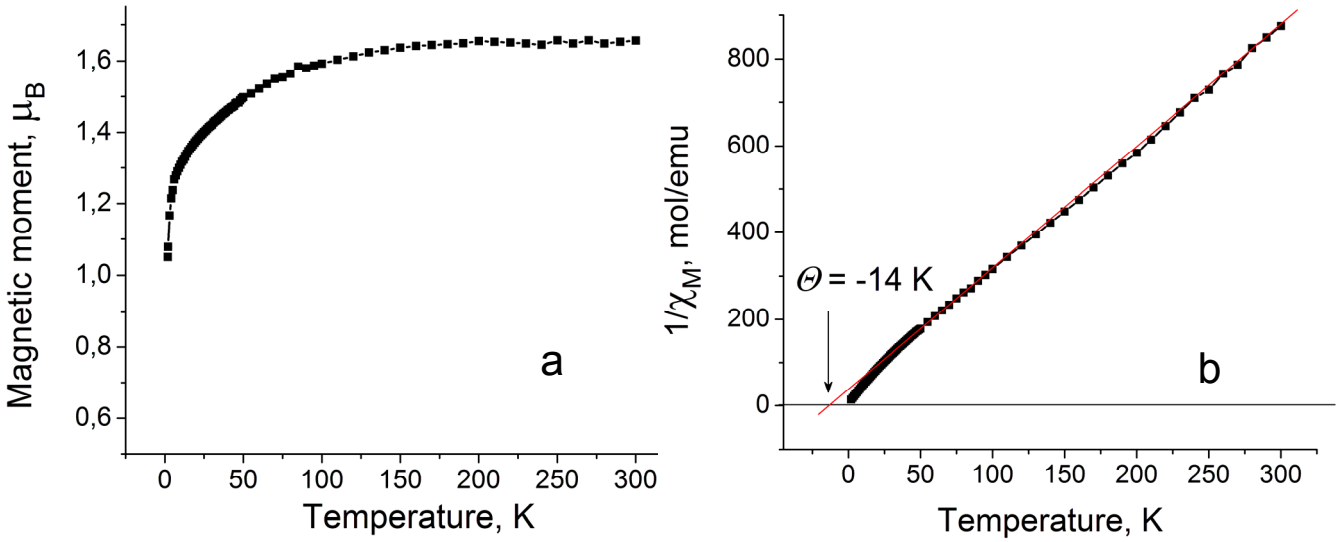

Fig. S4. Temperature dependences of effective magnetic moment (a) and reciprocal magnetic susceptibility of polycrystalline **2** (b).

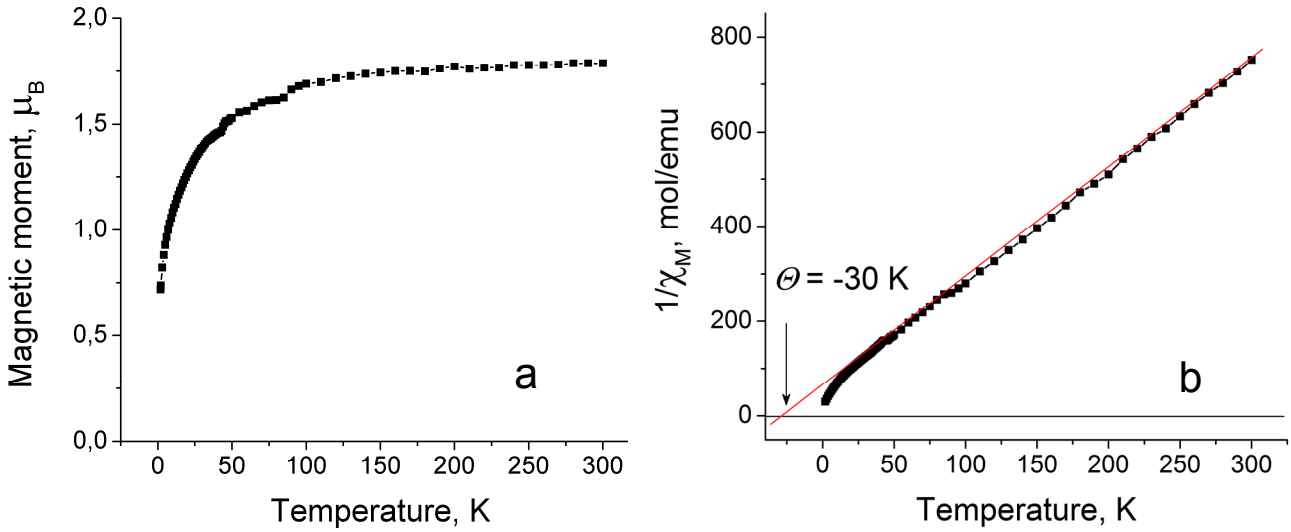

Fig. S5. Temperature dependences of effective magnetic moment (a) reciprocal magnetic susceptibility of polycrystalline **3** (b).

Data of EPR measurement for salt 2.

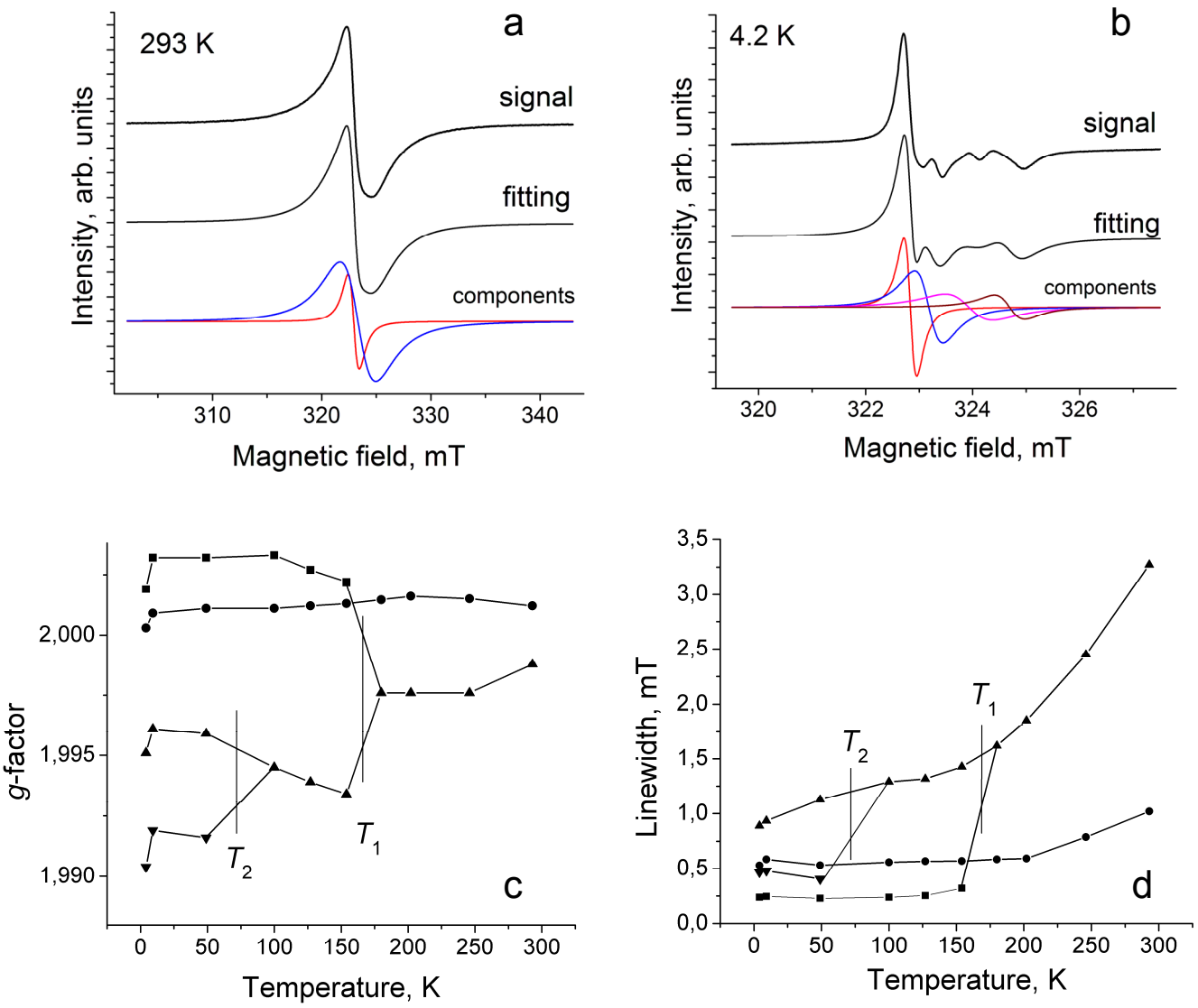

Fig. S6. EPR signal of polycrystalline **2** at 293 (a) and 4.2 K (b). The fitting of the signal by several Lorentzian lines is shown in middle and bottom; Temperature dependence of *g*-factor (c) and linewidth (d) of EPR signal of **2**. Temperature of splitting of EPR signal into three (T_1) and four (T_2) lines.

Fitting of the experimantal data by the Heisenberg models for antiferromagnetic coupling of spins.

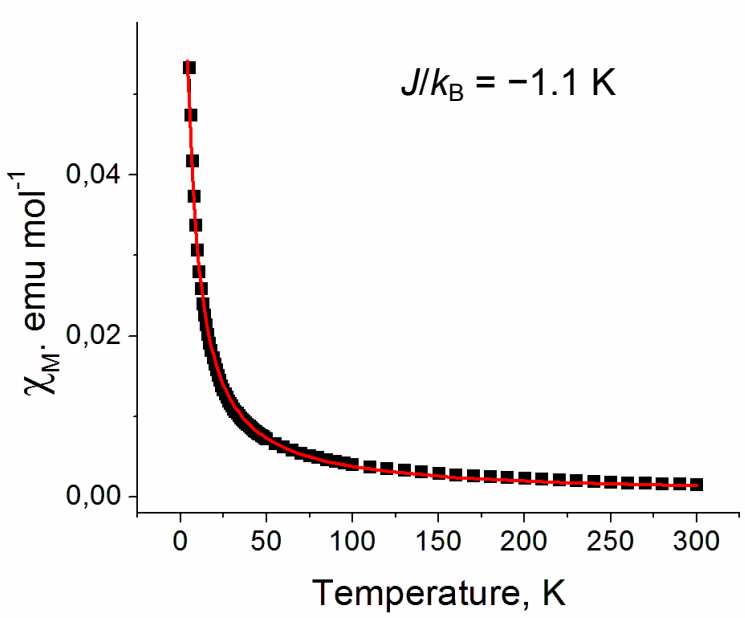

Fig. S7. Fitting of the experimental data (black squares) for polycrystalline salt **1** by the Heisenberg model for two-dimensional square antiferromagnetic coupling of spins[1] with exchange interaction J/k_B = − 1.1 K (red).

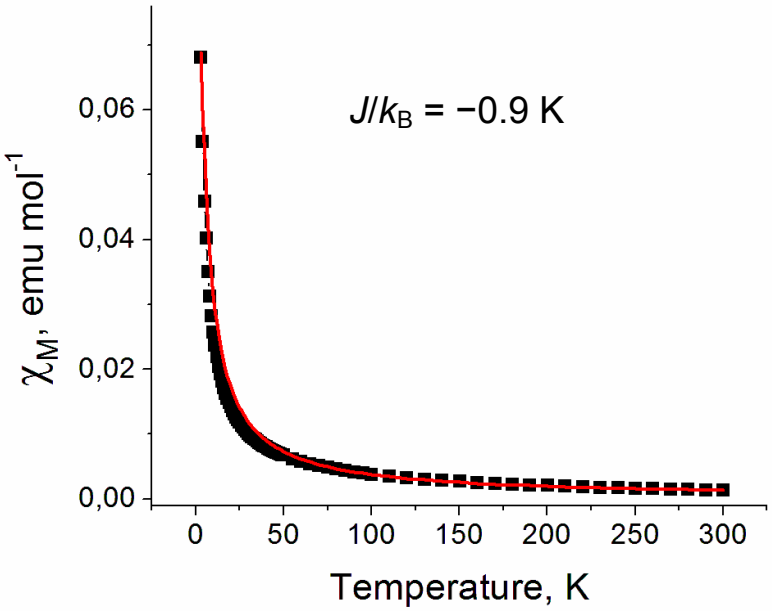

Fig. S8. Fitting of the experimental data (black squares) for polycrystalline salt **2** by the Heisenberg model for two-dimensional square antiferromagnetic coupling of spins[1] with exchange interaction J/k_B = − 0.9 K (red).

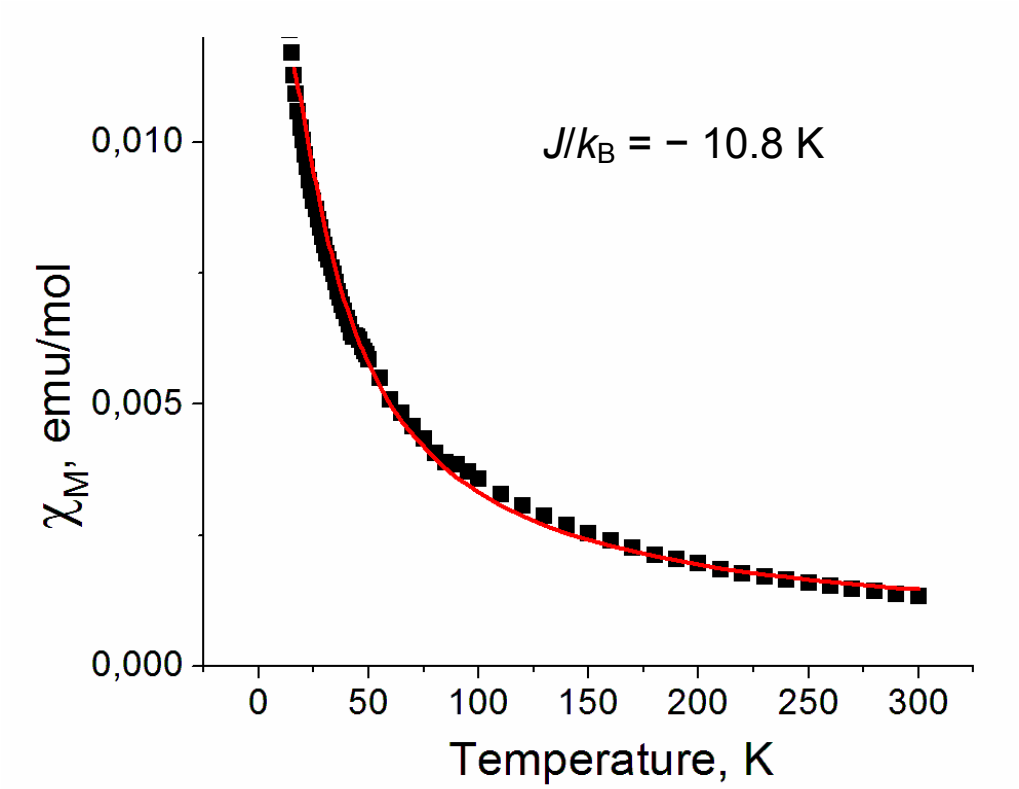

Fig. S9. Temperature dependence of molar magnetic susceptibility of **3** (black squares) and approximation of the data by the Heisenberg model for pairs of antiferromagnetically coupling spins[2] with exchange interaction of J/k_B = -10.8 K (red curve).

References.

1. M. E. Lines, *J. Phys. Chem. Solids* **1970**, *31*, 101–l16.
2. J. S. Smart, In Magnetism III, Eds by G. T. Rado, H. Suhl, Academic Press, NY, **1963**, p. 63.

Table S2. Symmetry (Sym), number of imaginary frequencies (Nimag), state, total and relative energies (E and ΔE), and $\langle S^2 \rangle$ values of $[Al(HFl–O^{-})(Pc^{\bullet 3-})]^{\bullet -}$ and $[Al(Fl{=}O^{\bullet -})(Pc^{\bullet 3-})]^{2\bullet -}$ calculated at the UM11/6-31+G(d,p) level of theory

	Sym	NImag	State	E / hartree	ΔE / K	$\langle S^2 \rangle$
$[Al(HFl–O^{-})(Pc^{\bullet 3-})]^{\bullet -}$	C_1	0	^2A	−2484.67848	−	0.822
$[Al(Fl{=}O^{\bullet -})(Pc^{\bullet 3-})]^{2\bullet -}$	C_1	0	^1A	−2484.07236	0	1.134
$[Al(Fl{=}O^{\bullet -})(Pc^{\bullet 3-})]^{2\bullet -}$	C_1	0	^3A	−2484.07222	46.6	2.136

Table S3. Charge and spin densities in the ^2A state of $[Al(HFl–O^{-})(Pc^{\bullet 3-})]^{\bullet -}$ and the ^1A state of $[Al(Fl{=}O^{\bullet -})(Pc^{\bullet 3-})]^{2\bullet -}$ by Mulliken and natural population analyses at the UM11/6-31+G(d,p) level of theory.

	Charge		Spin	
	MPA[a]	NPA[b]	MPA[a]	NPA[b]
$[Al(HFl–O^{-})(Pc^{\bullet 3-})]^{\bullet -}$				
Al	−0.201	2.020	−0.016	−0.002
Pc	−1.164	−2.258	1.009	1.000
HFl–O	0.365	−0.760	0.007	0.002
$[Al(Fl{=}O^{\bullet -})(Pc^{\bullet 3-})]^{2\bullet -}$				
Al	0.126	2.024	0.030	0.003
Pc	−1.702	−2.236	−0.999	−0.991
Fl=O	0.576	−0.787	0.969	0.988

[a] Mulliken population analysis. [b] Natural population analysis.

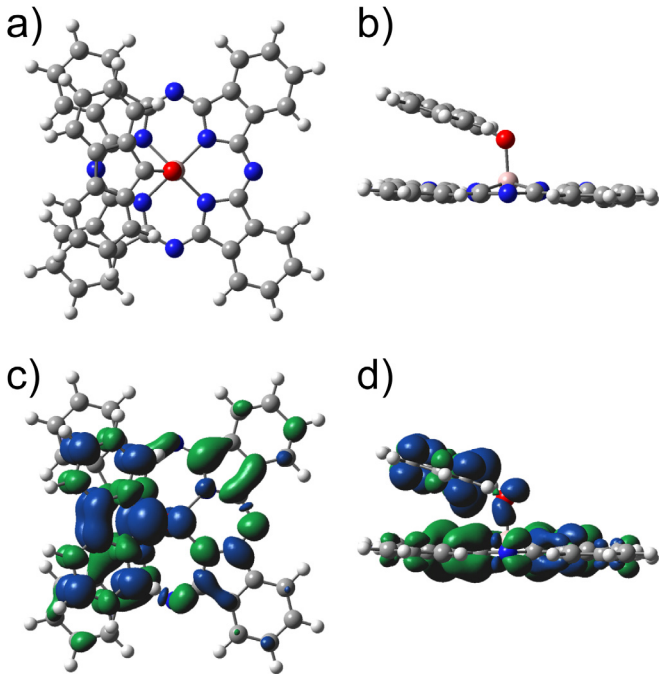

Figure S10. (a) Top and (b) side views of optimized structure in the ^{1}A state of $[Al(Fl{=}O^{\bullet-})(Pc^{\bullet 3-})]^{2\bullet-}$ at the UM11/6-31+G(d,p) level of theory. (c) Top and (d) side views of the spin density distribution, where the isosurface value is 0.0016 electron/au^{3}. The isosurfaces in blue and green denote the positive and negative spin density, respectively.